









Targeting Setdb1 in T cells induces transplant tolerance without compromising antitumor immunity

Received: 8 April 2023

Accepted: 1 April 2025

Published online: 15 May 2025



Xiaosheng Tan ^{1,2,10}, Xiangli Zhao^{1,10}, Zunsong Hu ^{3,4}, Ding-Sheng Jiang^{2,5}, Zhibo Ma¹, Lingjuan Sun¹, Jingzeng Wang¹, Xia Huang^{1,2}, Bin Xie^{1,2}, Mi Wu⁶, Min Ma⁷, Cong-Yi Wang ⁸, Shu Zhang ⁸, Li Chen ⁹, Zhishui Chen ^{1,2} , Gang Chen ^{1,2}  & Peixiang Lan ^{1,2} 

Suppressing immune responses promotes allograft survival but also favours tumour progression and recurrence. Selectively suppressing allograft rejection while maintaining or even enhancing antitumor immunity is challenging. Here, we show loss of allograft-related rejection in mice deficient in *Setdb1*, an H3K9 methyltransferase, while antitumor immunity remains intact. RNA sequencing shows that *Setdb1*-deficiency does not affect T-cell activation or cytokine production but induces an increase in Treg-cell-associated gene expression. Depletion of Treg cells impairs graft acceptance in *Setdb1*-deficient mice, indicating that the Treg cells promote allograft survival. Surprisingly, Treg cell-specific *Setdb1* deficiency does not prolong allograft survival, suggesting that *Setdb1* may function prior to *Foxp3* induction. Using single-cell RNA sequencing, we find that *Setdb1* deficiency induces a new Treg population in the thymus. This subset of Treg cells expresses less IL-1R2 and IL-18R1. Mechanistically, during Treg cell induction, *Setdb1* is recruited by transcription factor ATF and altered histone methylation. Our data thus define *Setdb1* in T cells as a hub for Treg cell differentiation, in the absence of which suppressing allograft rejection is uncoupled from maintaining antitumor immunity.

T cells, especially CD4⁺ T cells, are essential for transplant rejection^{1–4}. Upon recognizing a disparate major histocompatibility complex (MHC) or alloantigen, alloreactive T cells produce interferon (IFN)- γ and Fas ligand, which mediate cytotoxicity against the allograft⁵. This subset of CD4⁺ T cells has been identified as T helper 1 (Th1) cells. In order to target T-cell activation and differentiation, many immunosuppressive pharmacologic drugs have been applied to induce graft acceptance during organ transplant⁶. Unfortunately, suppressing T-cell activation and differentiation are associated with an increased risk of developing cancer or viral infection^{7–10}. Whether it is possible to selectively induce allograft tolerance while maintaining antitumor immunity remains unknown.

Regulatory T (Treg) cells, a specialized subpopulation of CD4⁺ T cells characterized as CD4⁺Foxp3⁺ T cells, are essential for maintaining self-tolerance, accomplished by suppressing T-cell proliferation and cytokine production¹¹. At the same time, in healthy individuals, immunity against tumors and viruses is normal¹². Therefore, approaches involving induction of Treg cells or enhancement of Treg cell function in vivo can lead to allograft tolerance. In 1990, CD4⁺CD25⁺ T cells were first reported to mediate transplant tolerance¹³. Since then, a number of experimental models and clinical trials have confirmed the role of Treg cells in suppressing alloreactive T-cell function and protecting transplanted grafts^{14–16}.

Recent advances have highlighted the heterogeneity of Treg cells, which is mainly a consequence of their plasticity and the microenvironment^{17,18}. Furthermore, in various inflammatory conditions there is often a dramatic loss of Treg function and Foxp3 transcription. In these Treg cells, conserved noncoding sequences (CNS) are highly demethylated, especially in CNS2, which is also termed the Treg-specific demethylated region (TSDR)^{19–21}. In addition to the methylation state of CpG dinucleotides, Foxp3 expression and Treg cell function are also dependent upon histone methylation^{22,23}.

SET domain bifurcated histone lysine methyltransferase 1 (Setdb1) is an H3K9 methyltransferase²⁴ that plays an important role in a variety of physiologic and pathologic processes because it methylates histone 3 lysine 9 (H3K9) residues. After T-cell activation, Setdb1 is dramatically induced to epigenetically regulate T-cell differentiation into distinct T-cell subsets such as Th1 and Th17 cells^{25,26}. Setdb1-deficient CD4⁺ T cells exhibit exacerbated Th1 priming in an IL-12-mediated Th1 differentiation assay, repressing a set of endogenous retroviruses (ERV) located in Th1 enhancers²⁵.

In this study, we investigate the role of Setdb1 in T cells and its impact on transplant tolerance and antitumor immunity. We find that Setdb1-deficient mice exhibit prolonged allograft survival without compromising tumor control. This effect is associated with enhanced Treg cell differentiation, which is independent of Foxp3 expression and involves a unique subset of regulatory T cells. Mechanistically, Setdb1 modulates histone methylation through ATF1 recruitment, influencing Treg stability in inflammatory environments. These findings highlight Setdb1 as a critical regulator of immune tolerance and suggest a potential therapeutic strategy for promoting transplant acceptance while preserving antitumor immunity.

Results

Setdb1-deficient T cells suppress allograft rejection but maintain anti-tumor immunity

To analyze whether Setdb1 in CD4⁺ T cells play a role in allograft rejection, we first generated T cell-specific Setdb1-knockout B6 mice (*Setdb1^{fl/fl}Cd4-Cre*, Supplementary Fig. 1). MHC-full mismatched BALB/c hearts were transplanted into *Setdb1^{fl/fl}Cd4-Cre* or *Setdb1^{fl/fl}* B6 mice (as a wild-type [WT] control). Consistent with other reports, WT B6 mice acutely rejected the allografts at days 7–8 ($n = 18$) (Fig. 1a). Interestingly, 13 of 18 *Setdb1^{fl/fl}Cd4-Cre* mice retained the BALB/c heart allografts for more than 100 days (Fig. 1a). Additionally, in the other five mice, graft failure was observed between 54 to 72 days post-transplant. As compared to those of WT mice, heart grafts from *Setdb1^{fl/fl}Cd4-Cre* mice had a nearly normal color and size, appearing very similar to hearts before transplantation (Fig. 1b), indicating that less lymphocytic infiltration and inflammation had occurred. Histology assays also indicated only minimal lymphocytic infiltration and vasculopathy (Fig. 1c). Our previous studies and others have shown that suppressing T-cell function with CTLA4-Ig does not inhibit chronic rejection (characterized as fibrosis at day 30 post-transplant in a mouse model; Fig. 1d). However, Setdb1 deficiency halted the progression of fibrosis (Fig. 1d, e). We further used a mouse skin graft model to test whether the anti-rejection effect in *Setdb1^{fl/fl}Cd4-Cre* mice is tissue-specific. The results showed that *Setdb1^{fl/fl}Cd4-Cre* mice had longer skin graft survival times and less severe transplant rejection (Supplementary Fig. 2). Thus, targeting Setdb1 in T cells suppressed both acute and chronic allograft rejection.

In contrast to suppressing allograft rejection, Setdb1-deficient T cells appropriately interfered with tumor progression. By using a B16 tumor-bearing mouse model, we discovered that tumor growth in *Setdb1^{fl/fl}Cd4-Cre* mice was not faster than that in WT mice and was even a little slower (Fig. 2a–c). Similar results were also observed in Hep1–6 (Fig. 2d–f) and MC38-based (Fig. 2g–i) mouse models. These data indicate that Setdb1-deficient T effector cells functioned as well as did WT T cells, even though the proportion of T cells in spleen and

allografts from *Setdb1^{fl/fl}Cd4-Cre* mice is lower than wild-type mice (Supplementary Fig. 3). When implanted with B16-OVA tumors, *Setdb1^{fl/fl}Cd4-Cre* mice showed comparable tumor volume, tumor mass, and the proportion and number of tumor-infiltrating OVA-specific CD8⁺ cells compared to WT mice (Supplementary Fig. 4). To confirm the role of T cells in controlling tumor growth, *Setdb1^{fl/fl}Cd4-Cre* mice were intraperitoneal injected with CD4 and CD8 depletion antibodies (200 µg/mouse), or NK cell depletion antibodies (200 µg/mouse), or the corresponding isotype three days before tumor implantation. Our data showed that tumor growth in *Setdb1^{fl/fl}Cd4-Cre* mice was faster when T cell depletion (Supplementary Fig. 5), but not with NK cell depletion, suggesting there is an effect of Setdb1 on T cell-mediated anti-tumor immunity.

Setdb1 deficiency enhances Treg cell priming

Because Setdb1 is an H3K9 methyltransferase that epigenetically regulates gene expression, we determined the gene expression of T cells from *Setdb1^{fl/fl}Cd4-Cre* and WT mice by using bulk RNA-seq, either activated by CD3 plus CD28 antibodies or not activated. Our data showed that naïve *Setdb1^{fl/fl}Cd4-Cre* CD4⁺ T cells exhibited Th1 features when compared to WT T cells (Fig. 3a). In response to stimulation, the expression of Th1-associated genes in activated *Setdb1^{fl/fl}Cd4-Cre* T cells was comparable to that in activated WT T cells (Fig. 3a). Also, we primed *Setdb1^{fl/fl}Cd4-Cre* and WT CD4⁺ T cells with IL-2 and IL-12 for 72 h to Th1 in vitro and found that T-bet, the key transcription factor in Th1 differentiation, was slightly lower in *Setdb1^{fl/fl}Cd4-Cre* CD4⁺ T cells than in WT CD4⁺ T cells (Supplementary Fig. 6a, b). Moreover, *Setdb1^{fl/fl}Cd4-Cre* CD4⁺ T cells produced a slightly lower levels of the cytotoxic cytokines IFN-γ and TNF-α (Supplementary Fig. 6c, d).

To assess the role of Setdb1 in Th1 cells infiltrating allografts, on day 7 we harvested the BALB/c heart grafts transplanted into *Setdb1^{fl/fl}Cd4-Cre* or WT mice and purified and analyzed the graft-infiltrated mononuclear cells. We found there was no difference in T-bet expression between *Setdb1^{fl/fl}Cd4-Cre* and WT CD4⁺ T cells infiltrating in allograft (Fig. 3b, c), although a little down-regulation of T-bet expression was observed in *Setdb1^{fl/fl}Cd4-Cre* CD4⁺ T cells from the spleen when compared to WT CD4⁺ T cells (Supplementary Fig. 7a, b). Moreover, no significant difference was found in between *Setdb1^{fl/fl}Cd4-Cre* and WT mice in terms of IFN-γ or TNF-α production by CD4⁺ T cells and CD8⁺ T cells infiltrating in the graft (Fig. 3d, e). Surprisingly, the serum IFN-γ was slightly increased in the *Setdb1^{fl/fl}Cd4-Cre* mice (Fig. 3f). We also observed comparable levels of cytotoxic effectors (e.g., perforin, granzyme B, and CD107a) in graft-infiltrating T-cell subsets between *Setdb1^{fl/fl}Cd4-Cre* and WT mice (Fig. 3d, g, h). Similar results were seen in the spleens of *Setdb1^{fl/fl}Cd4-Cre* and WT mice transplanted with BALB/c hearts for 7 days (Supplementary Fig. 7c–f). All these data suggest that Setdb1-deficient T cells suppressed allograft rejection, independent of Th1 priming.

The balance between co-stimulatory and inhibitory molecules determines T-cell activation, dysfunction, and exhaustion, which are critical to transplant rejection²⁷. We therefore next assessed the co-stimulatory and inhibitory molecules in graft-infiltrating and splenic T cells. No remarkable difference was seen in the frequency of CD69, CD25, OX40, GITR, DR3, CD44, CD62L, TIGIT, CTLA4, PD-1, TIM-3, or LAG-3-positive CD4⁺ T and CD8⁺ T cells infiltrating in grafts from *Setdb1^{fl/fl}Cd4-Cre* and WT mice (Supplementary Fig. 8a, b), although the mean fluorescence intensity of some was a little higher in *Setdb1^{fl/fl}Cd4-Cre* CD4⁺ T and CD8⁺ T cells when compared to WT tissues (Supplementary Fig. 8c, d). Similar results were observed in spleens from *Setdb1^{fl/fl}Cd4-Cre* and WT mice transplanted with BALB/c hearts (Supplementary Fig. 9). Hence, Setdb1-deficient T cells suppressed allograft rejection independent of T-cell dysfunction.

Because Treg cells contribute to graft acceptance, we next analyzed Treg cell-associated genes expressed in *Setdb1^{fl/fl}Cd4-Cre* or WT CD4⁺ T cells. First, we compared the Treg cell-related gene expression

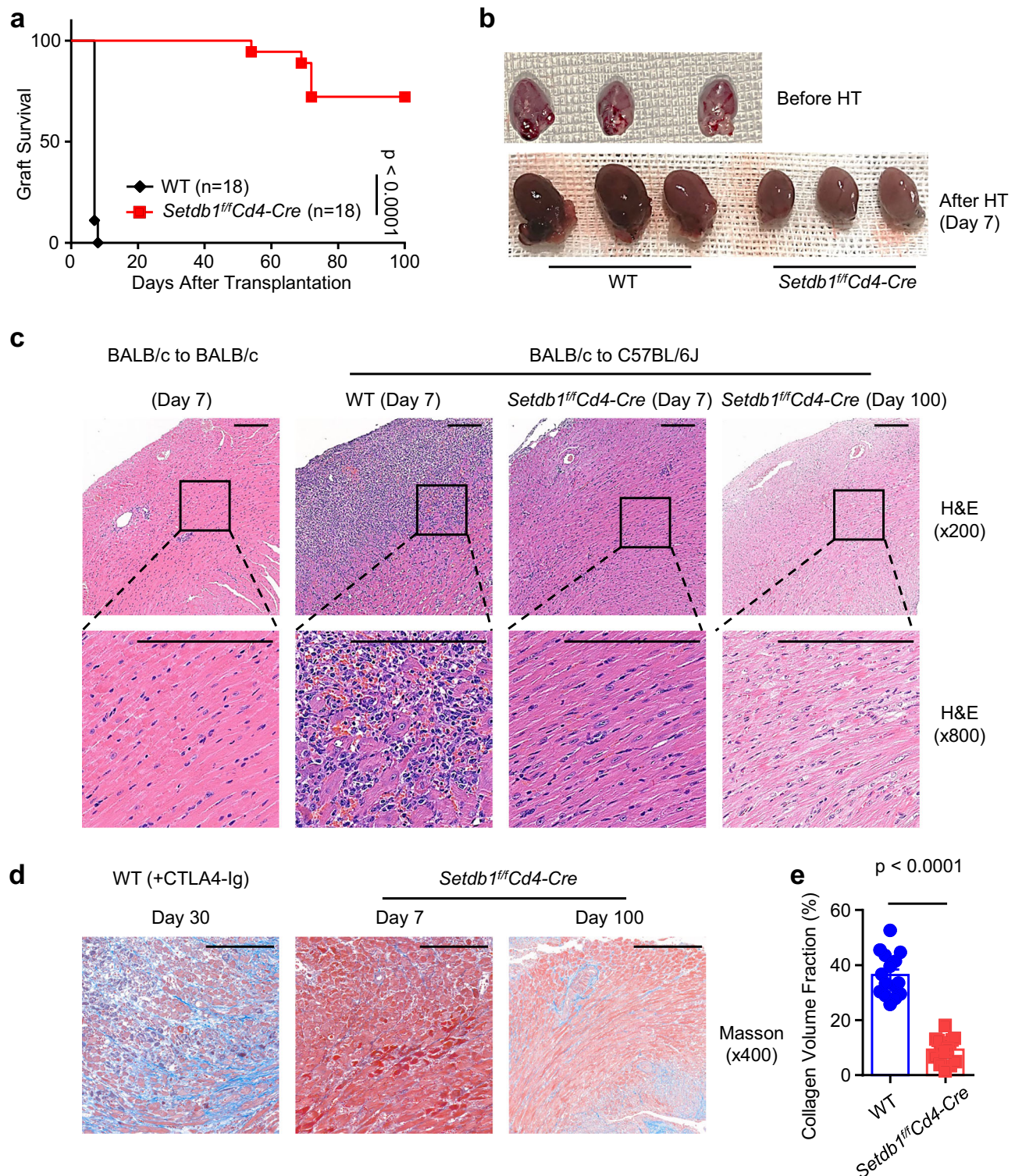


Fig. 1 | *Setdb1*-deficient T cells do not mediate heart allograft rejection. BALB/c hearts were transplanted into WT B6 and *Setdb1^{fl/fl}Cd4-Cre* mice. **a** Percentage of allograft survival after transplantation ($n = 18$). Log-rank (Mantel-Cox) test. **b** Representative images for hearts before transplantation (upper panel) and allografts harvested 7 days post-transplant from WT B6 and *Setdb1^{fl/fl}Cd4-Cre* mice (lower panel). **c** H&E-stained sections of heart allografts harvested from WT B6 recipients on day 7 post-transplant or from *Setdb1^{fl/fl}Cd4-Cre* recipients on day 7 or day 100 post-transplant. Representative images are shown. Scale bar: 200 μ m. **d, e** Masson trichrome staining of allograft sections from WT B6 recipients treated

with CTLA4-Ig on day 30 post-transplant, or from *Setdb1^{fl/fl}Cd4-Cre* recipients without treatment on day 7 or day 100 post-transplant. Representative images for each group (**d**) and bar graph of collagen volume fraction between WT B6 recipients (day 30) and *Setdb1^{fl/fl}Cd4-Cre* recipients (day 100). Scale bar: 200 μ m. **e** $n = 15$ for each group; 5 samples per group, three representative images of each sample were quantified and conducted data analysis. Unpaired Student's *t*-test (two-sided). Data are representative of three (**b–d**) independent experiments. Data are represented as means \pm SEM of at least three (**a, e**) independent experiments.

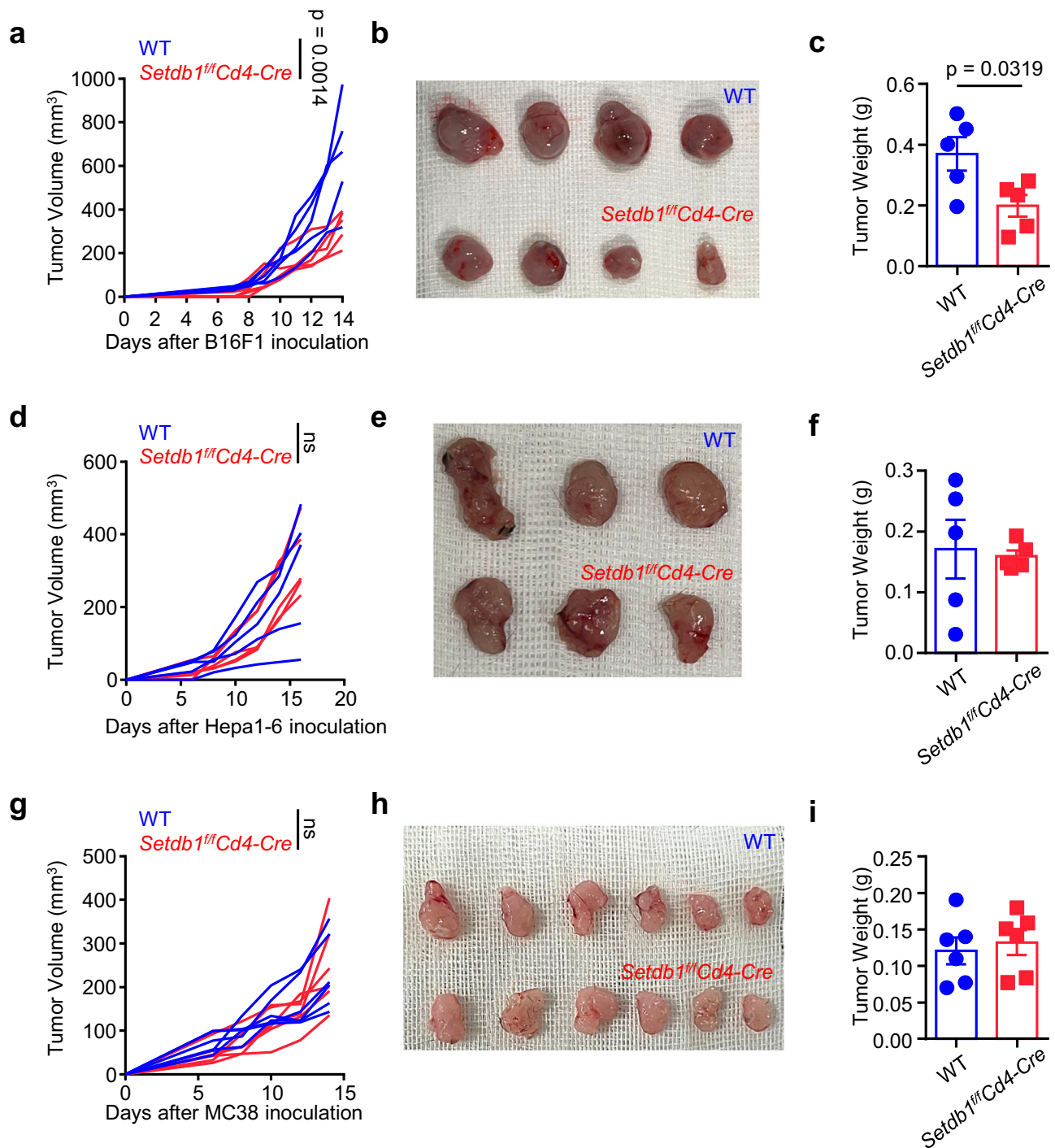
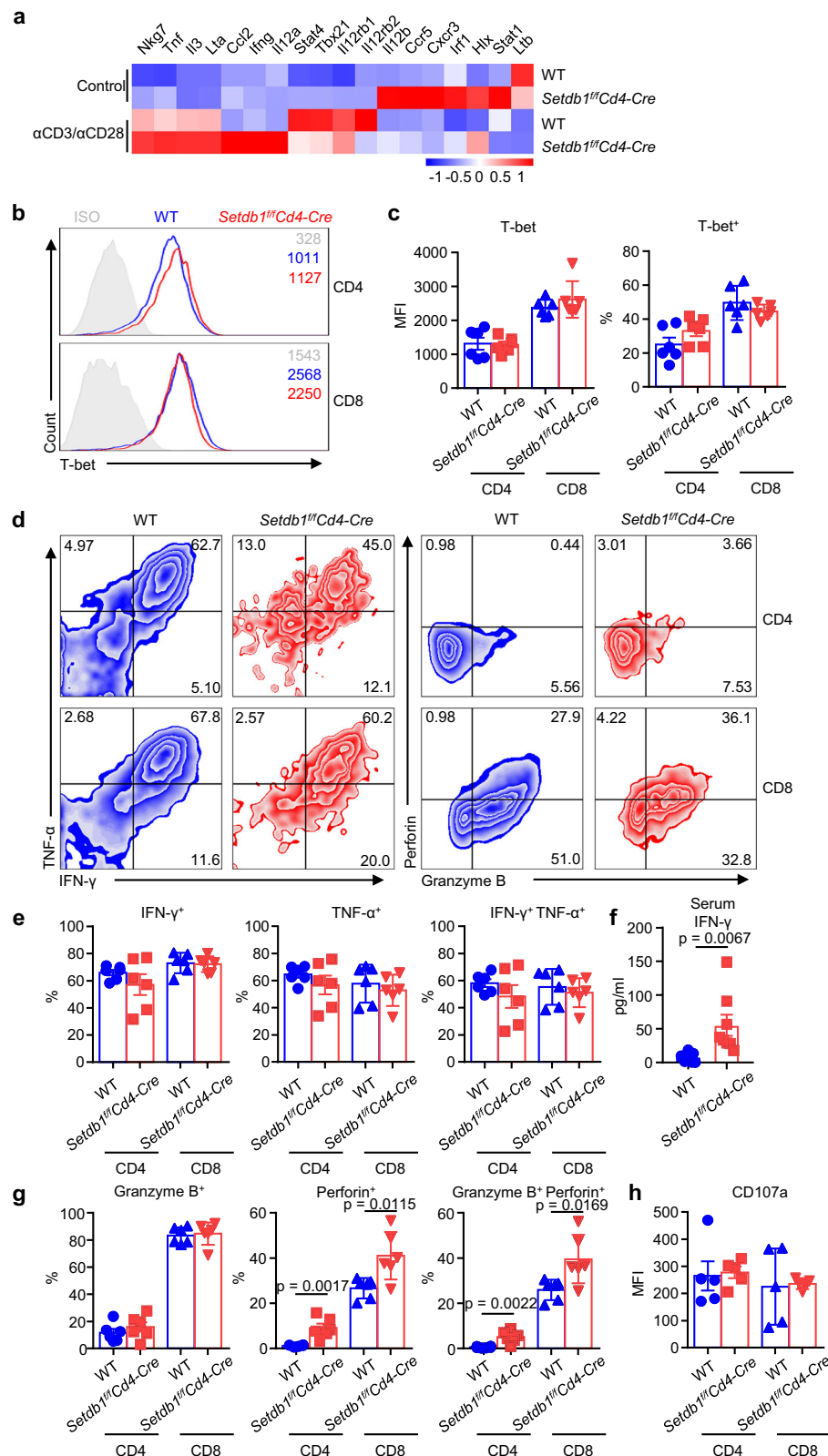


Fig. 2 | Mice with *Setdb1*-deficiency in T cells retain antitumor capacity. WT B6 and *Setdb1^{fl/fl}Cd4-Cre* mice were subcutaneously injected with 5×10^5 B16F1 melanoma cells (**a–c**), Hepa1-6 hepatoma cells (**d–f**), or MC38 colon cancer cells (**g–i**). **a, d, g** Xenograft tumor growth curve of different mice ($n = 5$ per group for B16F1 (**a**) and Hepa1-6 (**d**) xenograft tumor models. $n = 6$ per group for MC38 (**j**) xenograft

tumor models). ns, no significance; two-way ANOVA. **b, e, h** Representative pictures of tumors on day 14. **c, f, i** Tumor weights are shown as individual points ($n = 5$ or 6 per group). Unpaired Student's *t*-test (two-sided). Data are represented as means \pm SEM from a single representative experiment, with the experiment repeated independently three times.

in splenic CD4⁺ T cells from *Setdb1^{fl/fl}Cd4-Cre* and WT mice before and after heart transplantation (day 7). Our data show that many genes associated with Treg cells had a higher expression in *Setdb1^{fl/fl}Cd4-Cre* CD4⁺ T cells in the spleen than in the WT CD4⁺ T cells (Fig. 4a). On day 7 after heart transplantation, Treg cell-related gene expression was induced to a higher extent in splenic CD4⁺ T cells from *Setdb1^{fl/fl}Cd4-Cre* mice (Fig. 4a). To determine the frequency of Treg cells in the spleen and allograft, splenic and graft-infiltrating lymphocytes were

separated and assessed. Both before and after heart transplantation, the frequency of Treg cells was higher in the spleens from *Setdb1^{fl/fl}Cd4-Cre* mice (Fig. 4b, c). Moreover, Treg cells were much more plentiful in heart grafts from *Setdb1^{fl/fl}Cd4-Cre* mice than in WT mice (Fig. 4b, c). All these data indicate that *Setdb1* ablation promotes Treg cell differentiation. For further verification, we primed *Setdb1^{fl/fl}Cd4-Cre* and WT CD4⁺ T cells with IL-2 and TGF- β for 48 or 72 h against Treg cells in vitro. We found *Setdb1*-deficient CD4⁺ T cells exhibited enhanced



Treg priming (Fig. 4d, e). Interestingly, gene set enrichment analysis (GSEA) of splenic CD4⁺ T cells from WT B6 and *Setdb1*^{f/f}Cd4-Cre mice suggested that Treg cell-related genes were enriched in *Setdb1*-deficient CD4⁺ T cells (Fig. 4f). In addition, depletion of Treg cells with an anti-CD25 antibody offset the prolongation of allograft in *Setdb1*^{f/f}Cd4-Cre mice (Fig. 4g). Adoptive transfer CD25⁺ cells from *Setdb1*^{f/f}Cd4-Cre mice significantly prolonged the survival time of transplanted

hearts in WT mice and reduced transplant rejection (Supplementary Fig. 10). To further explore the role of *Setdb1* in Treg cells, we next generated *Setdb1*^{f/f}*Foxp3*-Cre mice. Surprisingly, the survival of heart grafts was not prolonged in the *Setdb1*^{f/f}*Foxp3*-Cre mice (Fig. 4h). Additionally, on day 7 posttransplant, we analyzed the proportion of Treg cells in the peripheral blood, lymph nodes, spleen, and grafts. The Treg cell proportions in the *Setdb1*^{f/f}*Foxp3*-Cre mice were similar to

Fig. 3 | Graft-infiltrated T cells retain Th1 phenotype and cytotoxicity in *Setdb1*-deficient mice. **a** Heatmap of Th1-related gene expression in splenic CD4⁺ T cells from WT B6 and *Setdb1*^{fl/fl}*Cd4-Cre* mice before and after anti-CD3/anti-CD28 stimulation (72 h). **b–h** WT B6 and *Setdb1*^{fl/fl}*Cd4-Cre* mice were transplanted with BALB/c hearts. Allografts and serum were harvested on day 7 post-transplant, and graft-infiltrated mononuclear cells were purified and analyzed. **b** Representative histograms showing T-bet expression in T-cell subsets, as determined by flow cytometry. **c** Mean fluorescence intensity of T-bet in T-cell subsets (left panel) and percentage of T-bet expression by T-cell subsets ($n = 6$ per group).

those in WT mice and lower than those in the *Setdb1*^{fl/fl}*Cd4-Cre* group (Supplementary Fig. 11a). In vitro Treg induction experiments also did not show that *Setdb1*^{fl/fl}*Foxp3-Cre* mice exhibited enhanced Treg priming (Supplementary Fig. 11b). Taken together, our data show that *Setdb1* may function before *Foxp3* expression.

Setdb1 deficiency promotes a new subset of Treg cells

Because *Foxp3* is induced in Treg cell differentiation in the thymus, we used single-cell sequencing to assess the effect of *Setdb1* in Treg cell differentiation (Table S1). A dimension-reduction method, Uniform Manifold Approximation and Projection (UMAP), was applied. The UMAP visualization showed that there were ten gene expression clusters (0–9) in thymocytes (Fig. 5a, Supplementary Fig. 12, Supplementary Fig. 13, Supplementary Data 1). Then a comparison of cell density for each cluster in the WT (WT-thymus) and *Setdb1*^{fl/fl}*Cd4-Cre* (KO-thymus) mice showed that cluster 4 was enriched in WT mice, whereas cluster 5 was enriched in *Setdb1*^{fl/fl}*Cd4-Cre* mice (Fig. 5b). Moreover, UMAP displaying pseudotime suggested that the transcriptional dynamics of cluster 4 and 5 were totally different (Fig. 5c, d). These two cell clusters had distinct transcriptional profiles (Fig. 5e, Supplementary Data 2). Cluster 4 showed characteristics of effector-like cells, with the expression of *Il1r2*, *Il18r1*, and *Irf2bp2*. Cluster 5, on the other hand, showed low levels of *Il1r2*, *Il18r1*, and *Irf2bp2* (Fig. 5e, f, Supplementary Data 2). These results indicated that cluster 5 Treg cells might be stable in an inflammatory micro-environment and maintain their function of regulating the immune response. We then tried to sort and transfer cluster 4 and 5 Treg cells in order to investigate their function. Unfortunately, there were too few of these cells to do the next adoptive transfer experiments. However, we found that *Il1r2* and *Il18r1* were reduced in *Setdb1*^{fl/fl}*Cd4-Cre* CD4⁺ T cells, suggesting that the Treg cell subset without expression of *Il1r2* and *Il18r1* exhibited a more stable regulatory function, causing more Treg cells to infiltrate into grafts from *Setdb1*^{fl/fl}*Cd4-Cre* mice (Fig. 4).

In the B16 tumor-bearing mouse model, we found that the frequency of Treg cells did not significantly change in the tumor tissue when *Setdb1* was specifically ablated in T cells (Fig. 5g, h). Interestingly, as compared to graft tissues, the tumor cells expressed less *Il18*, which interacted with and activated *Il18r*, which is highly expressed on WT Treg cells (Fig. 5i). Hence, Treg cells expressing *Il1r2* and *Il18r1* were unable to regulate the rejection when they entered the graft (where there was more *Il18* that activated *Il18r*), but the anti-tumor immunity was limited in the tumor tissues in which there was less *Il18*. Over-expression *Il18* in B16 cells can reduce the tumor size and the proportion of Treg cells within the tumor in tumor-bearing mice (Supplementary Fig. 14). *Setdb1* deficiency stimulated Treg cells to differentiate into a new subset expressing less *Il1r2* and *Il18r1* and retaining their function in the presence of inflammatory cytokines.

Setdb1 is recruited by ATF and promotes histone methylation in Treg cells

Our data show the important role of *Setdb1* in Treg cell differentiation and function, but the expression of *Setdb1* during Treg cell differentiation remains unknown. Our single-cell RNA-Seq data have shown that *Setdb1* is higher in cluster 4, which was enriched in WT mice

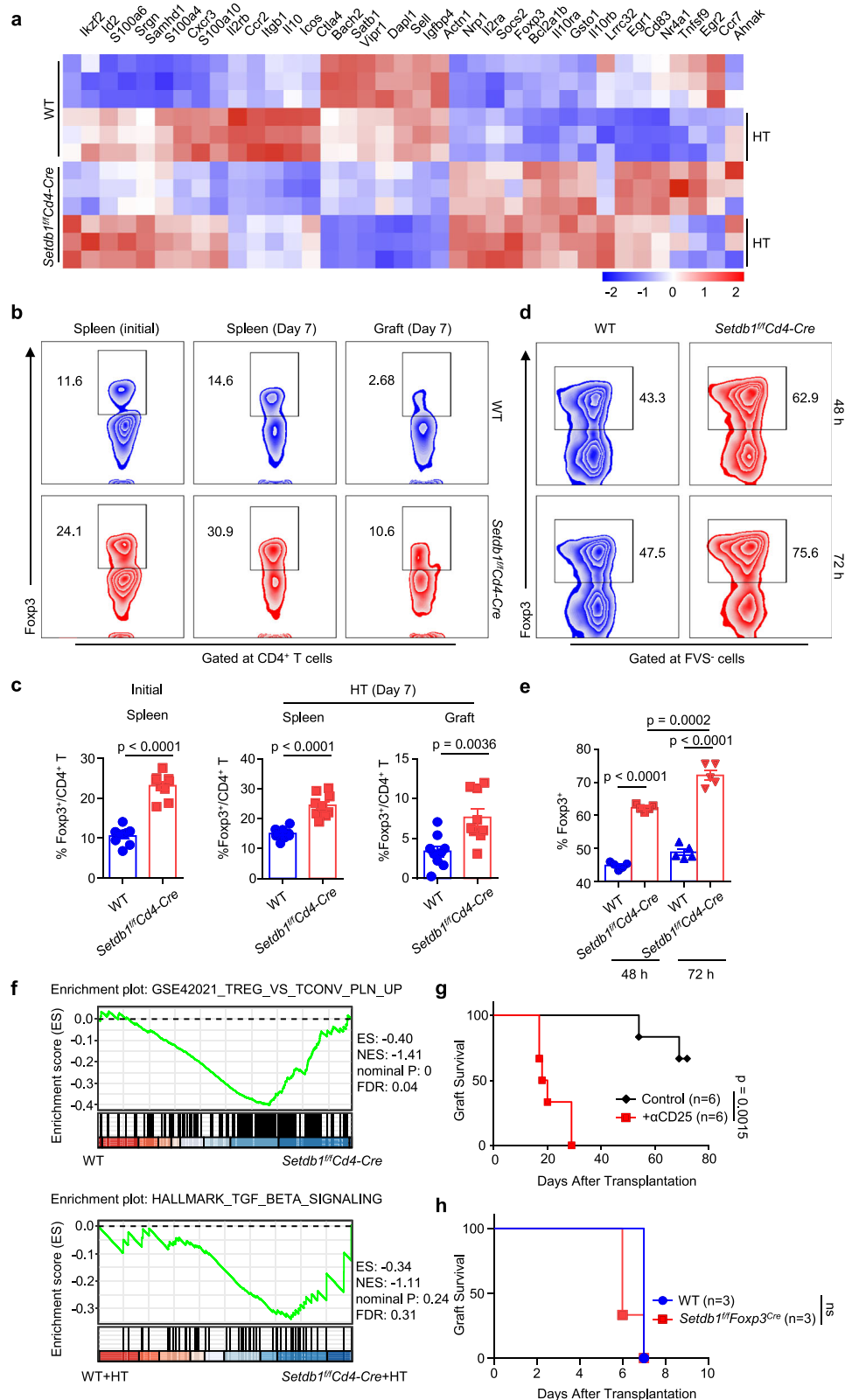
(Fig. 6a), but no significant difference was observed between clusters 4 and 5 in the expression of *Setdb2*, *Prmt1*, *Prmt5*, *Kdm5a*, or *Kdm5b*. To confirm this finding, we used transgenic *Foxp3*-GFP reporter mice to sort *Foxp3*-GFP Treg cells in the thymus and spleen (Fig. 6b). We found that there were few changes in *Setdb1* expression among CD25⁺ *Foxp3*-GFP⁺, CD25⁺ *Foxp3*-GFP⁺, and CD25⁺ *Foxp3*-GFP⁺ subpopulations from the thymus and spleen (Fig. 6c, d), indicating that the role of *Setdb1* was independent of its expression. To further explore the role of *Setdb1* in Treg cells, we applied IP-MS to identify the transcription factors that could interact with and recruit *Setdb1* to the specific histone that could be methylated by *Setdb1*. On the top of list was cyclic AMP-dependent transcription factor (ATF, Table S2), which is phosphorylated after TCR activation. This result was consistent with our IP assay showing that *Setdb1* bound to ATF1 (Fig. 6e). To confirm the role of ATF1, we used an inhibitor of PDE11(BC11-38) to activate the ATF1 signal pathway. We found that more *Setdb1* translocate into the nucleus when ATF1 is activated by the agonist (Fig. 6f, g). Then an assay of best-match TF motif to de novo motif sequence from the H3K9me3 CUT&Tag data showed that an ATF1-specific motif was enriched in WT CD4⁺ T cells but not in *Setdb1*^{fl/fl}*Cd4-Cre* CD4⁺ T cells (Fig. 6h). Additionally, when comparing the differential peaks between the WT B6 transplant group and the *Setdb1*^{fl/fl}*Cd4-Cre* transplant group, we found that the WT B6 group showed significant enrichment of many ATF-related motifs (Supplementary Fig. 15). As previously reported, zinc finger proteins (ZFP) were used as 'positive controls' for quality control purposes^{28,29}. All these data suggest that ATF1 is required to recruit *Setdb1* to specific histones.

Since *Setdb1* is a methyltransferase, we next tested the H3K4me3, H3K9me3, and H3K27me3 levels in Treg cells from WT and *Setdb1*^{fl/fl}*Cd4-Cre* mice. We observed that *Setdb1* ablation reduced the level of H3K4me3, H3K9me3, and H3K27me3 in Treg cells (Fig. 7a, b). Moreover, the induced Treg (iTreg) cells had higher levels of H3K4me3, H3K9me3, and H3K27me3 than did the natural Treg (nTreg) cells (Fig. 7c, d). Taken together, these data indicate that lowered histone methylation by targeting *Setdb1* is related to the stability of Treg cells. To further explore the effect of *Setdb1* on histone methylation in Treg cells, we performed CUT&Tag by using anti-*Setdb1* antibodies. A number of Treg cell-related genes such as *Foxp3*, *Il10*, *Il10ra*, *Il10rb*, and *Il2ra*, as well as the *Il1r1* and *Il18r2* loci, were enriched in *Setdb1* (Fig. 7e–g, Supplementary Fig. 16, Supplementary Data 3). These results were consistent with the CUT&Tag data using anti-H3K9me3 (Fig. 7e–g, Supplementary Fig. 16). Finally, *Setdb1*-mediated H3K9me3 depressed the expression of Treg cell-related genes (Fig. 7h). Given that *Setdb1* downregulates transposable elements (TE) in tumor cells³⁰, we compared the TE landscape between *Setdb1*-ablated and WT T cells. TEs were also activated in *Setdb1*-ablated T cells (Supplementary Fig. 17).

Organ allograft recipients have an increased risk of developing tumors, as a consequence of immunosuppression over their lifetimes^{31–33}. Calcineurin inhibitors, such as CsA/cyclophilin and FK506/FKBP, which are widely used in reducing graft rejection and autoimmunity, have been shown to suppress antiviral and antitumor immunity³⁴. Approaches for inducing allograft

Discussion

Organ allograft recipients have an increased risk of developing tumors, as a consequence of immunosuppression over their lifetimes^{31–33}. Calcineurin inhibitors, such as CsA/cyclophilin and FK506/FKBP, which are widely used in reducing graft rejection and autoimmunity, have been shown to suppress antiviral and antitumor immunity³⁴. Approaches for inducing allograft



tolerance while still retaining antitumor immunity need to be explored. Here, we have found that targeting *Setdb1* in T cells suppresses acute and chronic allograft rejection and controls tumor growth in tumor-bearing mouse models involving several tumor cell lines. We further show that *Setdb1* ablation promotes Treg cell differentiation via histone methylation, reprogramming the gene profiles in an ATF-dependent manner.

Treg cells are indispensable for preventing autoimmune inflammation and maintaining immunological tolerance. Impairing the development and function of Treg cells via the *Foxp3* gene mutation causes severe autoimmune disease in mice and humans^{35–37}. Indeed, numerous studies have shown that the frequency and function of Treg cells correlates with diverse autoimmune diseases³⁸. Therefore, Treg cell therapy using adaptive transfer is considered an all-purpose

Fig. 4 | Setdb1-deficiency Leads to An Increased Proportion of Regulatory T Cells. **a** Heatmap of regulatory T cell (Treg)-related gene expression in splenic CD4⁺ T cells from WT B6 and *Setdb1^{fl/fl}Cd4-Cre* mice before and after heart transplantation (day 7). The WT B6 without heart transplantation group served as a control. **b** Representative zebra plots of splenic and graft-infiltrating Treg cells in WT B6 and *Setdb1^{fl/fl}Cd4-Cre* mice before and after heart transplantation (day 7). **c** Percentage of splenic and graft-infiltrating Tregs before and at 7 days after transplant ($n = 9$ per group). Unpaired Student's *t*-test (two-sided). **d, e** Naïve splenic CD4⁺ T cells were purified from WT B6 and *Setdb1^{fl/fl}Cd4-Cre* mice, then stimulated with anti-CD3/anti-CD28 in the presence of IL-2 (10 ng/ml) and TGF- β

(10 ng/ml) for 48 or 72 h. **d** Representative zebra plot of foxp3 expression determined by flow cytometry. **e** Percentage of Foxp3-expressing cells at 48 h and 72 h after being cultured in Treg-polarizing conditions ($n = 5$ per group). Unpaired Student's *t*-test (two-sided). **f** Gene set enrichment analysis (GSEA) of splenic CD4⁺ T cells from WT B6 and *Setdb1^{fl/fl}Cd4-Cre* mice before and at 7 days post-transplant. **g** BALB/c heart graft survival in *Setdb1^{fl/fl}Cd4-Cre* mice with/without anti-CD25 injection ($n = 6$). Log-rank (Mantel-Cox) test. **h** BALB/c heart graft survival in WT B6 and *Setdb1^{fl/fl}Foxp3-Cre* mice ($n = 3$). ns: no significance; log-rank (Mantel-Cox) test. Data are representative of at least four (**b, d**) independent experiments. Data are shown as means \pm SEM of at least three (**c, e, g, h**) independent experiments.

solution for autoimmune disease and allograft rejection. Unfortunately, the adoptively transferred Treg cells compromise the immune response and become ineffectual in an inflammatory setting, as a result of the down-regulation of Foxp3 expression and methylation of TSDR³⁹. Here, we found that targeting Setdb1 can increase the frequency of Treg cells in vivo, especially in the allograft. Consequently, the allografts survived for a long time, without acute or chronic rejection. Indeed, we observed some fibrosis formation in the grafts of *Setdb1^{fl/fl}Cd4-Cre* mice 100 days post-transplantation, but the severity was much lower compared to the positive control mice with chronic rejection. This indicates that Treg cells in *Setdb1^{fl/fl}Cd4-Cre* mice suppress rejection responses, which are related to fibrosis. Surprisingly, Setdb1 ablation did not suppress effector T-cell function. Setdb1-deficient T cells produced the cytotoxic cytokines IFN- γ and TNF- α , almost as WT T cells do, leading to a control of the tumor growth in a tumor-bearing mouse model. Additionally, most *Setdb1^{fl/fl}Cd4-Cre* mice with heart transplants can induce transplant tolerance. However, in the skin transplant model, while *Setdb1^{fl/fl}Cd4-Cre* mice can extend the survival time of skin grafts, long-term immune tolerance was not observed. This is likely related to differences in Setdb1-dependent Treg function and immune regulation at different tissue sites. Further research is needed to elucidate these details.

Recent single-cell sequencing data have revealed that Treg cells show a high degree of heterogeneity⁴⁰. Subsets of Treg cells with unstable Foxp3 expression or lacking a suppressive function are not true Treg cells. Comparison of cell density for each cluster in WT and *Setdb1^{fl/fl}Cd4-Cre* mice showed that cluster 4 was enriched in WT mice, whereas cluster 5 was enriched in *Setdb1^{fl/fl}Cd4-Cre* mice. Moreover, Cluster 4 showed characteristics of effector-like cells with the expression of Il1r2, Il18r1, and Irf2bp2, which are activated by cytokines in inflammatory microenvironments. In *Setdb1^{fl/fl}Cd4-Cre* mice, a new subset of Treg cells was induced, characterized as Foxp3⁺Il1r2⁺Il18r1⁺. Accumulating evidence has shown that IL1 β , elevated in inflammatory settings, can promote the differentiation of Treg cells to Th17 cells and enhance the accumulation of inflammatory cells⁴¹. Our data have shown that the graft-infiltrating Treg cells are less common than in the spleen. However, in Setdb1-deficient mice, there were significantly more graft-infiltrating Treg cells than in the WT mice. All these data indicate that cluster 5 might represent true Treg cells and be stable in inflammatory settings. Our data show, nevertheless, that Setdb1 ablation enhances Treg cell function and promotes allograft survival.

Recent studies have revealed that Setdb1 alters T-cell function and mediates T-cell development and differentiation in response to various stimuli. After OX40 activation, Setdb1 has been shown to be recruited to the IL-17 locus by RelB and then to repress the expression of IL-17 and decrease Th17 cell function²⁶. In an IL-12-mediated Th1 differentiation assay, Setdb1 is enriched in endogenous retroviruses (ERV) near Th1 gene enhancers and suppresses Th1 differentiation²⁵. Here, we also found ERVs were activated in Setdb1 ablation T cells. But we also found Setdb1 bound to CNS of Foxp3, which directly regulates Foxp3 expression. By IP assays, we have shown that Setdb1 binds ATF1, and ATF1 activation increases the translocation of Setdb1 to the nucleus. ATF1, which belongs to the activator protein-1 (AP-1) family, is involved

in mediating proliferation and differentiation of T cells during TCR activation. Interestingly, by means of Foxp3 reporter mice, TCR signaling has been shown to induce Foxp3 gene transcription. Furthermore, in mice knocked-in with TCRs of defined antigen specificity, Treg cell differentiation and function have been found to require more specificity than when these processes involve conventional T cells. Beyond the thymic development of Treg cells, peripheral Treg (pTreg) cells are also induced by strong agonists. All these findings suggest that TCR controls Treg cell differentiation and function^{42,43}. Importantly, in organ transplantation, allorecognition by TCR and allogeneic MHC, with or without bound peptides, is stronger than recognition by TCR and neoantigen in tumor tissues. This might be the reason that targeting Setdb1 shows different effects on rejection and antitumor immunity.

There are limitations to our study that need to be mentioned. Specifically, the precise role of the new Treg cell subset in allograft rejection remains to be further clarified. The frequency of this cellular subpopulation in mouse is very low, making functional analysis particularly challenging. Unfortunately, there were insufficient numbers of these cells to perform sorting and adoptive transfer to further confirm their immunosuppressive function. Furthermore, we applied anti-CD3 antibody to stimulate T cells instead of peptides. However, considering the more specificity of antigens Treg cell needed for differentiation and function, it is better to using specific peptides for further confirmation the role of Setdb1 and ATF1 in T cell development and differentiation. In our experiments on the ATF1 pathway, the PDE11 inhibitor we used may have effects independent of ATF-1, so these results should be interpreted with caution. A more specific ATF1 agonist or inhibitor is needed for future studies. Furthermore, while we confirmed the important role of IL-18 in Treg cell stability, our study cannot definitively conclude that IL-18 is the sole factor influencing Treg differentiation. There may be other factors, such as IL-10 or other unidentified elements, that contribute to this process. Although we demonstrated that Treg cells from *Setdb1^{fl/fl}Cd4-Cre* mice exhibit strong immunosuppressive capacity in preventing graft rejection, the precise pathways through which they exert their immunosuppressive effects require further exploration in future studies. Additionally, we observed the binding of SETDB1 and H3K9me3 near the Foxp3 gene and other Treg-related genes. However, SETDB1-dependent H3K9me3 is often concentrated around ERV-encoded enhancers distal to target genes. Therefore, it is currently challenging to determine which mechanism plays a dominant role. Further research is needed to unravel this mystery.

Collectively, we have found that targeting Setdb1 raises the frequency of Treg cells and promotes allograft survival. However, in our hands, Setdb1 deficiency does not affect T-cell activation or cytokine production, enhancing the anti-tumor function of the T cells. Our findings further suggest an approach for tolerance induction and hint that targeting Setdb1 may have greater potential than use of traditional immunosuppressants.

Methods

Study design

The aim of this study was to explore a target in T cells that suppressing allograft rejection while maintaining antitumor immunity. The goal

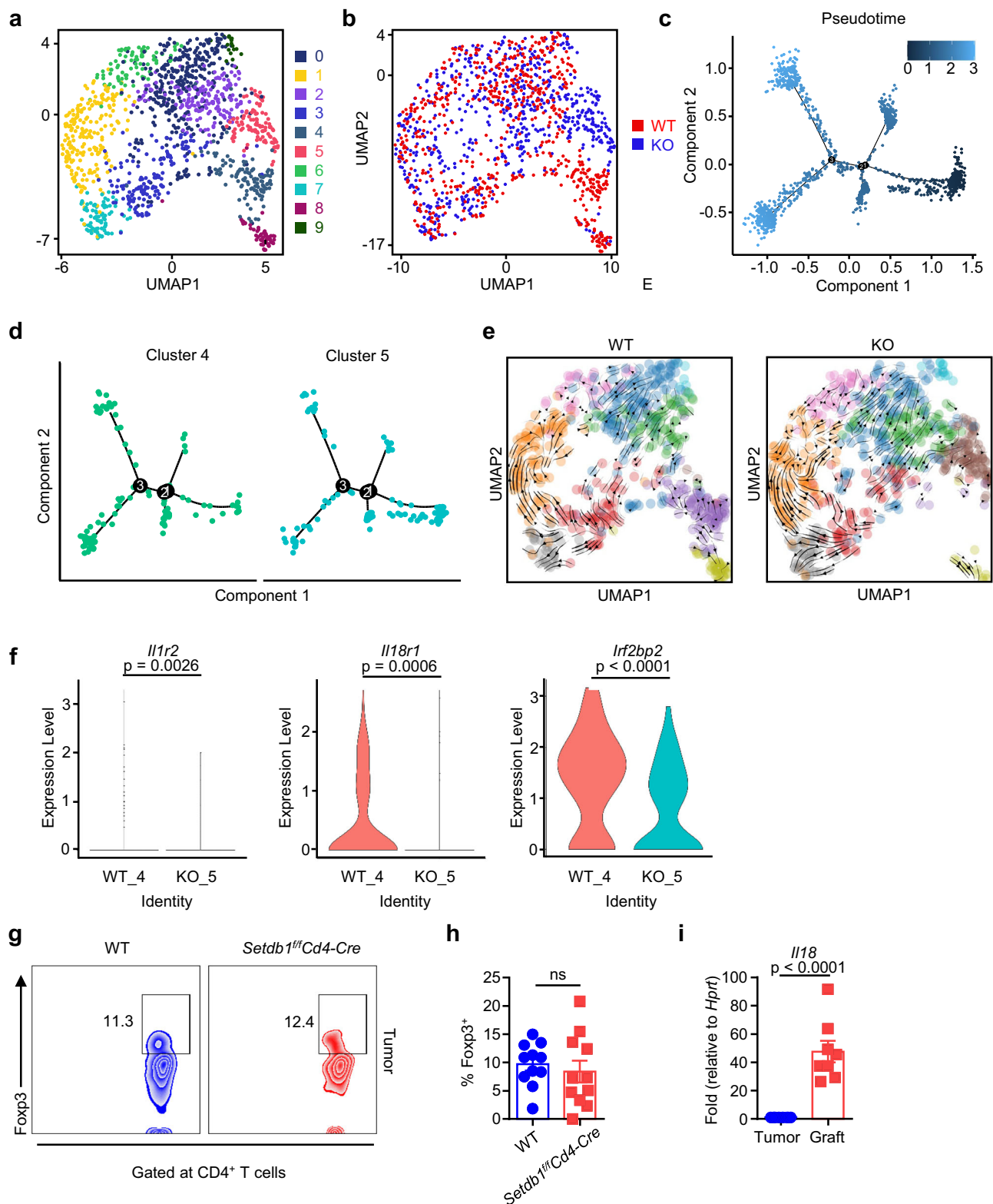
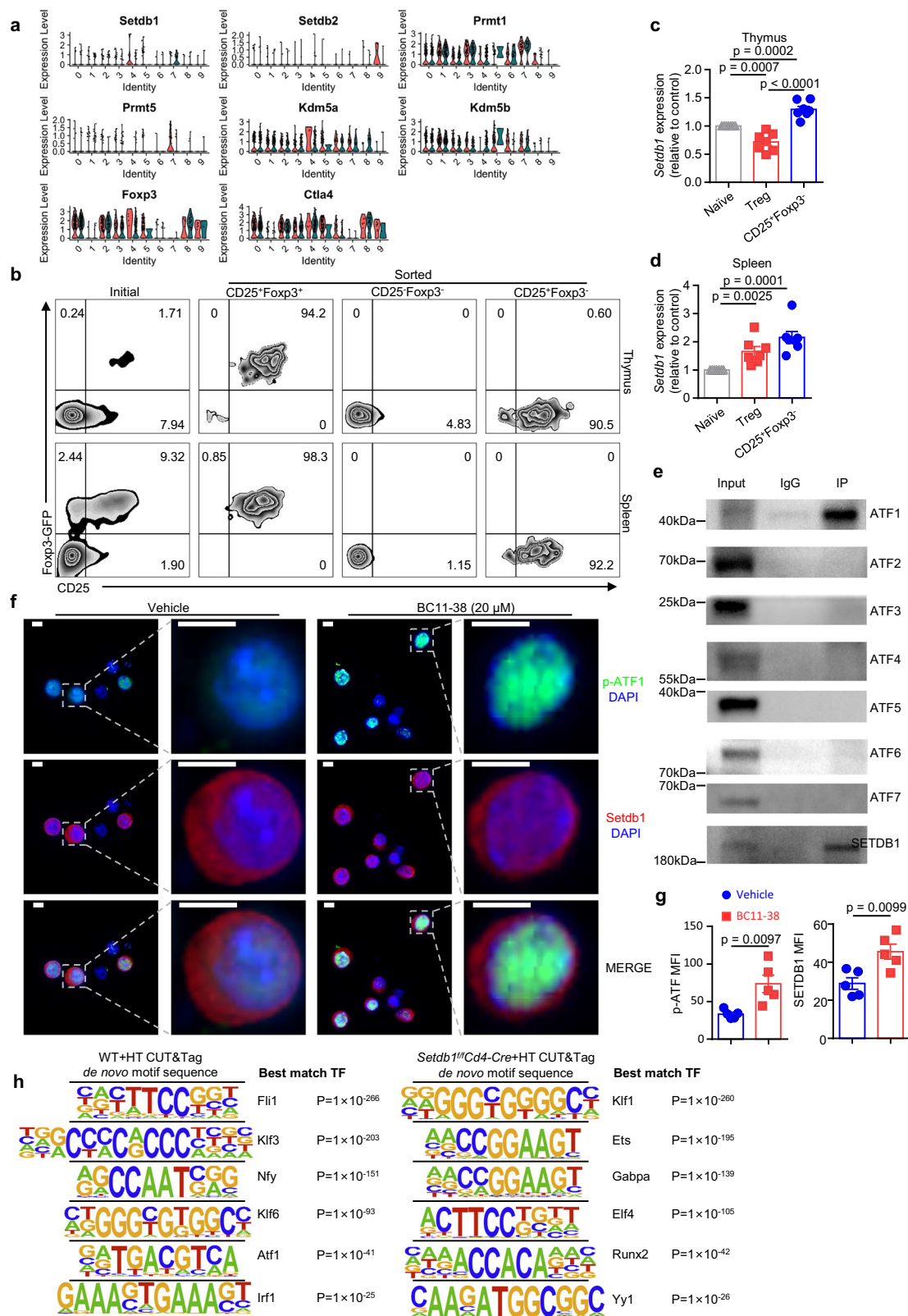


Fig. 5 | *Setdb1* Controls Treg Cell Development in the Thymus. **a–f** Thymocytes from WT B6 and *Setdb1^{fl/fl}Cd4-Cre* mice were processed for single-cell RNA sequencing (scRNA-seq). **a** Ten gene expression clusters (0–9) projected on a UMAP of the scRNA-seq libraries. **b** Comparison of cell density for each cluster in WT B6 (WT, red) and *Setdb1^{fl/fl}Cd4-Cre* (KO, blue) mice. **c** UMAP embedding displaying the thymocyte colored by pseudotime. **d** Projection of clusters 4 and 5 according to the position of their cells on the pseudotime. **e** Velocities derived from the dynamic model for Treg development, projected onto UMAP-based embedding. **f** Gene expression of *Il1r2*, *Il18r1*, and *Irf2bp2* in cluster 4 from WT B6 and

cluster 5 from *Setdb1^{fl/fl}Cd4-Cre* mice (two-sided). **g** Representative zebra plot of intratumoral Treg cells in WT B6 and *Setdb1^{fl/fl}Cd4-Cre* mice at day 14 post-inoculation. **h** Percentage of intratumoral Treg cells from WT B6 and *Setdb1^{fl/fl}Cd4-Cre* mice ($n = 11$ per group). **i** Comparison of *Il18* levels for xenograft B16F1 melanoma (14 days post-inoculation) and BALB/c allografts (3 days post-transplant) ($n = 8$ per group). Data are representative of at least four independent experiments. Data are shown as means \pm SEM of at least three independent experiments. ns, no significance; unpaired Student's *t*-test (two-sided). See also Table S1, Supplementary Data 1, and Supplementary Data 2.



was achieved by using *Setdb1^{fl/fl}Cd4-Cre* mice; a cardiac allograft rejection model; a chronic rejection model; and tumor models. For mechanistic study, we compared allograft survival time between *Setdb1^{fl/fl}Cd4-Cre* mice and *Setdb1^{fl/fl}Foxp3-Cre* mice. Also, we performed several biochemistry experiments, such as bulk and single-cell RNA-seq, CUT&Tag assay, co-IP assay, flow cytometric analysis, immunofluorescence, quantitative real-time reverse transcription PCR (RT-PCR)

analysis, ex vivo Treg cell induction, etc. All data points generated were included in the analysis. For in vitro and in vivo studies, at least three independent experiments were performed. Besides, for in vivo studies, mice were randomly assigned for experiments. The sample size is specified in each figure legend. The experiments were performed unblinded. The key resources of this research were listed in Supplementary Data 4.

Fig. 6 | ATF1 is required to recruit Setdb1 to specific histones. **a** Gene expression in clusters from WT B6 (green) and *Setdb1^{fl/fl}Cd4-Cre* mice (red). **b–d** CD4⁺CD25⁺Foxp3-GFP⁺ naïve T cells, CD4⁺CD25⁺Foxp3-GFP⁺ Treg cells, and CD4⁺CD25⁺Foxp3-GFP⁺ subsets were purified by fluorescence-activated cell sorting from WT B6 thymocytes and splenocytes. **b** Representative zebra plots for cell subset proportions before and after sorting. **c, d** Setdb1 expression in naïve CD4⁺ T cells, Treg cells, and CD25⁺Foxp3⁺ subsets from thymus (**c**) and spleen (**d**) as measured by real-time quantitative PCR ($n = 7$ per group). Unpaired Student's *t*-test (two-sided). **e** Immunoblot analysis of ATF1-7 in cell lysates immunoprecipitated

with anti-Setdb1 or IgG from WT-naïve CD4⁺ T cells stimulated with anti-CD3/anti-CD28 for 72 h. **f** Co-localization of p-ATF1 and Setdb1 in in vitro-induced Treg cells treated with or without BC11-38 (20 μ M). Scale bar: 5 μ m. **g** The fluorescence intensities of p-ATF1 or SETDB1 within the cell nucleus are shown ($n = 5$ per group). Unpaired Student's *t*-test (two-sided). **h** Best match TF motif to de novo motif sequence was assessed from H3K9me3 CUT&Tag. Data are representative of at least three (**b, e, f**) independent experiments. Data are shown as means \pm SEM of at least three (**c, d, g**) independent experiments. Also see Table S2 and Supplementary Data 3.

Mice

Specific pathogen-free C57BL/6JNifdc (stock number: 219) and BALB/c mice (stock number: 211) were purchased from Charles River Laboratories (Beijing, China). *Cd4-Cre* transgenic mice (stock number: 022071) were purchased from Model Organisms (Shanghai, China), and genotyped. *Foxp3-GFP* mice [C57BL/6-Tg(Foxp3-GFP)90Pkraj/J, stock number: 023800] and *Foxp3-Cre* mice [B6129S-Tg(Foxp3-EGFP/icre)1ajbs/J, stock number: 023161] were obtained from Jackson Laboratory (Bar Harbor, ME, USA). The *Setdb1^{fl/fl}* mice were generated by the CRISPR-Cas9 system (GemPharmatech), and were backcrossed with *Cd4-Cre* transgenic mice or *Foxp3-Cre* mice, to generate mice with selective deletion of Setdb1 in T cells (*Setdb1^{fl/fl}Cd4-Cre*) or in Tregs (*Setdb1^{fl/fl}Foxp3-Cre*). To generate the floxed allele, two gRNAs (gRNA1: TGCGTCCGACGTTTACCTC, gRNA2: ATGAAGCCTGCAGGAATAA) targeting introns flanking the critical exon(s) were used, and a donor vector containing loxP sites was introduced for homology-directed repair. The Cas9 protein, gRNAs, and donor DNA were microinjected into C57BL/6 zygotes. Positive founders were confirmed by PCR and sequencing. All mice were maintained under controlled conditions (22 °C, 50% humidity, 12 h light/dark cycle, with lights on at 7:00 AM). Mice were euthanized by CO₂ inhalation followed by cervical dislocation, in accordance with institutional animal care guidelines.

In vivo cell depletion

T cell or NK cell was depleted by administering 200 μ g of depleting antibodies i.p. weekly beginning three days prior to tumor implantation as indicated: CD4⁺ T cells with anti-CD4 (clone GK1.5, BioXCell), CD8⁺ T cells with anti-CD8 α (clone 2.43, BioXCell), NK cells with anti-NK1.1 (clone PK136, BioXCell). For CD25⁺ cell depletion, purified CD25 antibody was administered 100 μ g per mice i.p. twice weekly, beginning three days prior to transplantation.

Transplantation procedures

Heart transplantation in mice was performed according to a previously described method⁴⁴. In brief, hearts from BALB/c donors were transplanted into 8- to 10-week-old male WT B6 or *Setdb1^{fl/fl}Cd4-Cre* recipient mice. The pulmonary artery and aorta of the donor heart were cut open, the remaining heart vessels were tied off, and the heart was removed. The chest cavity of an anesthetized recipient mouse was opened with a midline incision, and blood flow via the abdominal aorta and inferior vena cava was interrupted by ligation with 6-0 silk thread. Incisions were made in the recipient's abdominal aorta and inferior vena cava to allow for anastomosis to be performed with the donor heart aorta and donor pulmonary artery, respectively. Anastomosis was made by 11-0 sutures running continuously; The 6-0 silk thread was removed, and the abdomen was then closed by 5-0 sutures in two layers. Heart graft survival was monitored daily by palpation, and the day of complete cessation of heartbeat was considered the day of rejection. Allografts were harvested for analysis at the time of rejection or at the indicated time points.

Skin transplantation in mice was performed as follows. BALB/c mice were euthanized, and their tails were swabbed with 70% ethanol. A 1.0 \times 1.0 cm² section of tail skin was removed from the donor. Recipient mice were anesthetized with isoflurane, and hair on their backs was removed with depilatory cream. The shaved area was cleaned with

70% ethanol and allowed to dry. A 1.0 \times 1.0 cm² area of back skin was removed from the recipient mice to create a graft bed. The donor skin graft was placed into the graft bed and stitched at the corners. The mice were then wrapped with bandages and placed in an incubator until they could move freely.

Histological examination and immunofluorescent staining

Grafts were fixed in 4% formaldehyde and dehydrated with xylene, absolute ethyl alcohol, and 75% alcohol, then embedded in paraffin wax. Four micron-thick sections were cut. Graft histological changes were revealed by hematoxylin & eosin (H&E) staining. Fibrosis degree was determined by Masson trichrome staining. T-cell infiltration into grafts was estimated by staining with anti-CD3 primary antibody according to a standard protocol (Servicebio).

For determination of p-ATF1/Setdb1 expression and intracellular co-localization in iTregs treated with or without p-ATF1 agonist (BC11-38), a cell pellet-based immunofluorescent staining was applied. In brief, cells were first fixed in 2% formaldehyde for 15 min and washed with PBS, and pellets were collected. A 2–4% liquid agarose was used for coating the pellets. After the agarose solidified, the clump was dehydrated with xylene, absolute ethyl alcohol, and 75% alcohol, then embedded in paraffin wax. Immunofluorescent staining was performed according to a standard protocol (LabEXTM).

Cell lines and tumor models

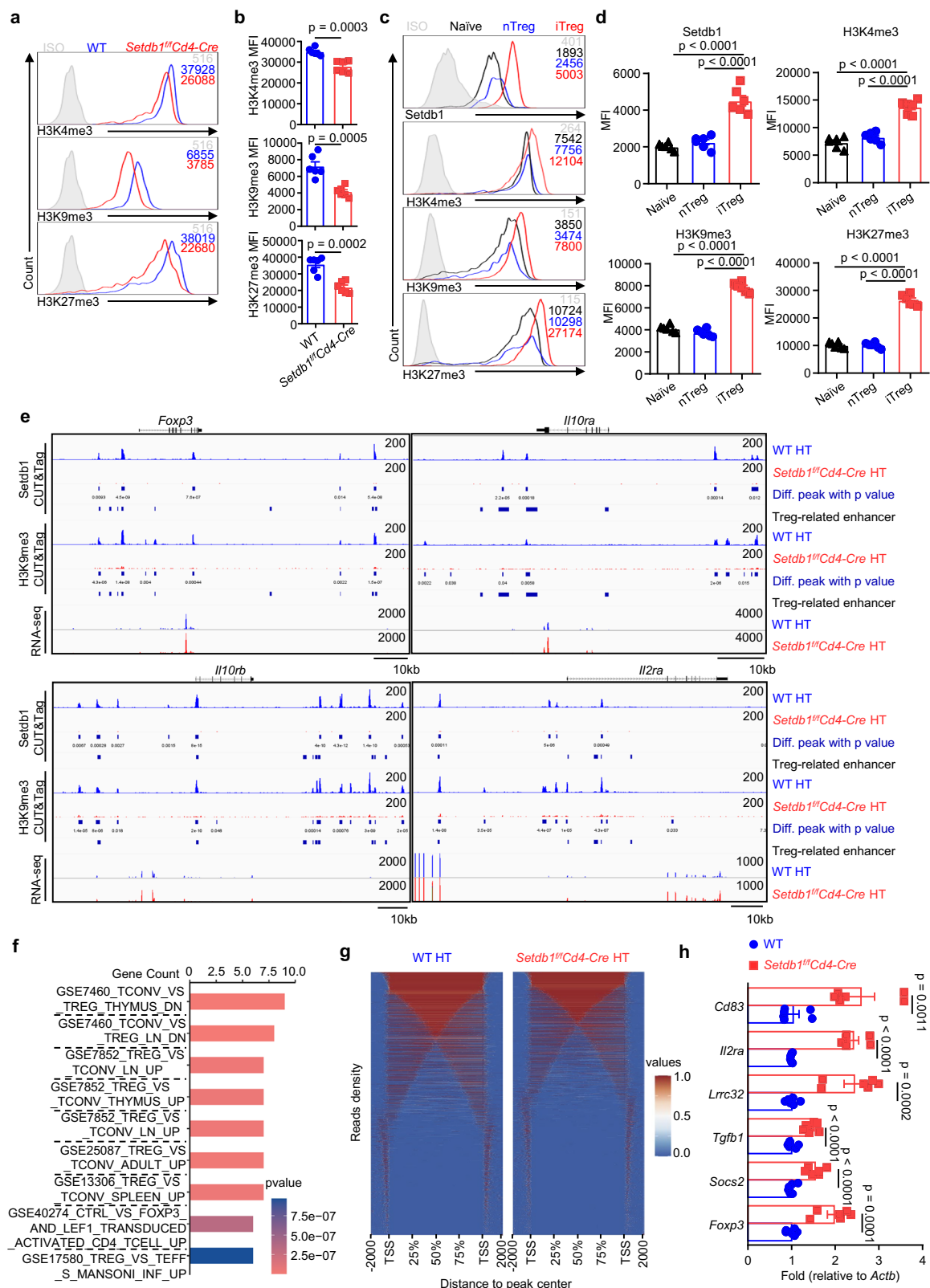
B16F1, Hepa1-6, and MC38 were purchased from the China Center for Type Culture Collection, and cultured in RPMI1640 medium (Gibco) plus 10% FBS (Yeasen Biotechnology Co., Ltd., Shanghai, China) and 1% penicillin/streptomycin (New Cell & Molecular Biotech Co., Ltd., Shanghai, China).

For the tumor model, 5 \times 10⁵ tumor cells were injected subcutaneously into the right flank of mice, and tumor growth was measured by multiplying the length of the tumor by the width. Tumors in mice were monitored continuously for 7 days starting on day 7 of tumor loading. For in vivo depletion T cells, anti-CD4 and anti-CD8 depletion antibodies or their corresponding isotype (BioXCell) were given at 200 μ g per mouse at 3 days before tumor implant. To verify the effect of IL-18 on Treg cells and its anti-tumor efficacy, we transfected pCMV-IL18 or empty vector to B16F1, followed by puromycin screening, eventually obtaining the target cells.

Isolation of graft-infiltrating mononuclear cells, tumor-infiltrating mononuclear cells, splenocytes, and thymocytes

Mice bearing heart allografts were euthanized on day 7. Grafts were removed and cut into pieces, washed with PBS, and then digested at 37 °C for 30 min in DMEM containing 100 ng/mL type II collagenase (SigmaAdrich) before being pressed through a 70- μ m filter (Biosharp). The collected cells were washed, and graft-infiltrating mononuclear cells were purified by density gradient centrifugation in a 38% Percoll solution (GE Healthcare).

For purification of tumor-infiltrating mononuclear cells, tumor-bearing mice were euthanized on day 14, and tumors were isolated from the surrounding tissue. Tumors were washed with PBS and then digested at 37 °C for 30 min in DMEM containing 100 ng/mL type IV



collagenase (SigmaAldrich) before being pressed through a 70- μ m filter (Biosharp). The collected cells were washed by PBS, followed by density gradient centrifugation in 38% Percoll solution (GE Healthcare).

Purified splenocytes were prepared by homogenization with a syringe, followed by passage through a 0.1-mm sterile nylon mesh and density gradient centrifugation in mouse 1 \times lymphocyte separation

medium (Dakewe). Thymocytes were prepared by pressing thymus tissue through a 70- μ m filter.

Flow cytometry

Cells were stained with various fluorochrome-conjugated antibodies, followed by analysis with a BD Celesta cell analyzer (BD Biosciences). Intracellular staining for Foxp3, T-bet, H3K4me3, H3K9me3,

Fig. 7 | *Setdb1* deficiency leads to a reduction in H3K9me3 and reinforces Treg-related gene expression. **a** Representative histogram for H3K4me3, H3K9me3, and H3K27me3 levels in Tregs from WT B6 and *Setdb1*^{fl/fl}*Cd4-Cre* mice. **b** Mean fluorescence intensity of H3K4me3, H3K9me3, and H3K27me3 in Tregs from WT B6 and *Setdb1*^{fl/fl}*Cd4-Cre* mice ($n = 6$ per group). Unpaired Student's *t*-test (two-sided). **c** Representative histograms for *Setdb1*, H3K4me3, H3K9me3, and H3K27me3 expression in naïve CD4⁺ T cells, natural Tregs, and induced Tregs. **d** Mean fluorescence intensity of *Setdb1*, H3K4me3, H3K9me3, and H3K27me3 in naïve CD4⁺ T cells, natural Tregs, and induced Tregs ($n = 6$ per group). Unpaired Student's *t*-test (two-sided). **e** *Setdb1* CUT&Tag, H3K9me3 CUT&Tag, and RNA-seq tracks at Treg-related gene locus. Differential peaks in WT B6 mice with heart transplantation, compared to *Setdb1*^{fl/fl}*Cd4-Cre* mice, are displayed along with their respective *P*-

values. Tracks indicating enhancers associated with Treg cells, as identified in EnhancerAtlas 2.0, are included as a reference track. See also Supplementary Fig. 16. **f** Bar plot showing the *Setdb1* CUT&Tag enrichment results based on the msigdb-C7 database from the corresponding genes determined by upregulated differential peaks in WT B6 with heart transplantation when compared to *Setdb1*^{fl/fl}*Cd4-Cre* mice. Hypergeometric distribution test, correction method: Benjamini–Hochberg (one-sided). **g** Differential peaks across each Treg cell enhancer (two-sided). **h** mRNA expression of Treg-related genes in splenic CD4⁺ T cells from WT B6 and *Setdb1*^{fl/fl}*Cd4-Cre* mice with heart transplantation (day 7) ($n = 6$ per group). Unpaired Student's *t*-test (two-sided). Data are representative of at three (**a**, **c**) independent experiments. Data are shown as means \pm SEM of at least three (**b**, **d**, **h**) independent experiments.

H3K27me3, and *Setdb1* was performed using the Transcription Factor Buffer Set (BD Biosciences). Intracellular staining of IFN- γ , TNF- α , granzyme B, and perforin was performed according to the Intracellular Flow Cytometry Staining Protocol (Biolegend). For detection of intracellular IFN- γ and TNF- α , a cell-stimulation cocktail containing PMA/ionomycin and brefeldin A (eBioscience) was used to stimulate splenocytes for 4 h. Cytokine levels in mouse serum were measured with a CBA kit for mouse Th1/Th2/Th17 cytokines according to the manufacturer's instructions. Data were analyzed with FlowJo software (TreeStar). Gating strategies have been provided in Supplementary Fig. 18.

Cell sorting

To induce Foxp3⁺ or T-bet⁺ T cells in vitro, naïve CD4⁺ T cells were sorted by magnetic bead separation by using Naïve CD4⁺ T Cell Isolation Kit (Miltenyi). To assess the gene expression in thymocyte subsets, thymocytes from *Foxp3-GFP* reporter mice were depleted of CD8⁺ cells, followed by staining with PE-labeled anti-CD4 and APC-labeled anti-CD25 antibodies. T-cell subsets were sorted with a high-speed cell sorter FACSaria III (BD Biosciences).

In vitro T-cell stimulation

To activate T cells, naïve CD4⁺ T cells were added at 2×10^5 cells/well to anti-CD3 (5 μ g/ml)-precoated 96-well round-bottom tissue culture plates (Corning); the culture medium contained 1 μ g/ml soluble anti-CD28 mAb. For polarization of CD4⁺ T cells in vitro, cultures were supplemented with various cytokines (PeproTech, Rocky Hill, NJ) and small-molecule inhibitors (MCE). For Th1 polarization, naïve CD4⁺ cells were activated in the presence of 10 ng/ml mouse IL-2 and 10 ng/ml mouse IL-12. For Treg polarization, naïve CD4⁺ cells were activated in the presence of 10 ng/ml human TGF- β 1 and 10 ng/ml mouse IL-2. For Th2 polarization, naïve CD4⁺ cells were activated in the presence of 10 ng/ml mouse IL-2 and 50 ng/ml mouse IL-4. For Th17 polarization, naïve CD4⁺ cells were activated in the presence of 50 ng/ml mouse IL-6 and 10 ng/ml human TGF- β . To promote ATF1 phosphorylation, BCII-38 was used at a concentration of 20 μ M. CD4⁺ T cells cultured for different numbers of days were collected and analyzed by flow cytometry, immunoblotting, immunofluorescent staining, quantitative real-time PCR, co-immunoprecipitation, RNA-seq, and CUT&Tag.

Quantitative RT-PCR

Total RNA was extracted from T cells using a RNeasy200 kit (Qiagen), and cDNA was synthesized using the PrimeScript RT Reagent Kit (Takara). The expression of genes of interest and of the HPRT control was assessed by PCR using SYBR Green mix (Yeastar). Transcript levels of target genes were calculated as the ratio of target gene expression to β -actin expression. Fold changes in target gene expression were analyzed by StepOne Software (Applied Biosystems) using the delta/delta CT method.

Immunoblot analysis

Protein extracts were resolved by SDS-PAGE, transferred onto an Immobilon membrane, and analyzed by immunoblotting with the antibodies indicated. Horseradish peroxidase-linked antibody to rabbit immunoglobulin G (ThermoFisher) and horseradish peroxidase-linked antibody to mouse immunoglobulin G (ThermoFisher) were used as secondary antibodies. Protein expression was detected by chemiluminescence.

Co-immunoprecipitation assay

CD4⁺ T cells from WT mice were stimulated by anti-CD3/anti-CD28 for 72 h. Cells (4×10^6 cells) were collected in NETN lysis buffer. Subsequently, the cell lysate was incubated with anti-*Setdb1* (1:50, CST) or control antibody at 4 °C for 2 h, followed by incubation with Magna ChIP™ Protein A+G Magnetic Beads (Merck) overnight. Beads were collected by centrifugation and washed 4 times with IP lysis buffer. Proteins were resolved in PBS and analyzed by immunoblotting.

Bulk RNA sequencing

Total RNA was extracted from purified CD4⁺ T cells with TRIzol (Invitrogen). Total RNAs (2 μ g) were used for stranded RNA sequencing library preparation by means of a Stranded mRNA Library Prep Kit from DR08502 (Bioyigene) according to the manufacturer's instructions. The library products corresponding to 200–500 bp were enriched, quantified, and finally sequenced on DNBSEQ-T7. The gene expression profiles of CD4⁺ T cells from WT B6 and *Setdb1*^{fl/fl}*Cd4-Cre* mice after various treatments were determined by RNA-Seq data analysis (Bioyigene). In brief, raw sequencing data were first filtered by FastQC; low-quality reads were discarded, and adaptor sequences were trimmed. After quality filtering, each sample had 49.5–67.5 million clean reads. Clean reads from each sample were mapped to the *Mus musculus* GRCm38 reference genome using hisat2. Significantly differentially expressed transcripts were screened by applying the criteria $FC \geq 2$ or ≤ -2 and P -value < 0.05 . The RNA-seq data, entitled “Transcriptome RNA-seq analysis for WT and *Setdb1* kco mice CD4⁺ T cells before and after stimulation or transplantation” were deposited in the Sequence Read Archive (SRA) with BioProject number PRJNA843698.

Cleavage under targets and tagmentation (CUT&Tag)

CUT&Tag was performed using the Hyperactive Universal CUT&Tag Assay Kit. The sequencing process was outsourced to Novogene Co., Ltd. Briefly, after harvesting, CD25⁺ enriched T cells were counted and divided into groups of 200,000 cells each. The cells were centrifuged at 600g for 5 min at room temperature. Each sample was resuspended in 100 μ l of pre-cooled NE Buffer, mixed gently, and incubated on ice. Following incubation, the cells were centrifuged again at 600g for 5 min at room temperature, and the pellets were resuspended in 100 μ l of wash buffer.

Next, 10 μ l of Concanavalin A-coated magnetic beads, pre-activated at room temperature, were added to each sample and incubated for 10 min. The unbound supernatant was removed, followed by an overnight reaction between the H3K9me3 group sample and anti-H3K9me3 antibodies (1:50, Proteintech), as well as between the SETDB1 group sample and anti-SETDB1 antibodies (2 μ g, Proteintech) in Antibody Buffer at 4 °C.

After washing, the bound antibodies were reacted with secondary antibodies and then incubated with pA/G-Tnp Pro (0.04 μ M). Next, the samples were fragmented with TTBL, followed by the addition of 10% SDS and DNA spike-in to each sample. To extract the genomic DNA, DNA Extract Beads Pro were activated and added to each sample. The extracted DNA fragments were amplified by PCR with indexing primers (Vazyme, TD202), and the library was purified using VAHTS DNA Clean Beads (Vazyme, N411).

Adapter sequences and low-quality reads in the raw CUT&Tag data were filtered using BBDuk (version 38.44). The filtered reads were then aligned to the mouse mm10 reference genome using Bowtie2 (version 2.4.2) with the parameters “--local --very-sensitive --no-mixed --no-discordant --phred33 -I 10 -X 700.” Duplicate reads were removed with the MarkDuplicates function in GATK (version 4.2.0). Coverage (bigWig) files were generated from the resulting BAM files using the bamCoverage tool in deepTools. Peak calling was performed using MACS2 (version 2.2.7.1) with the parameters “--keep-dup all --broad --broad-cutoff 0.05.” Finally, quantitative differences in binding and corresponding p-values were determined using MANorm (version 1.3.0). Binding motifs were obtained using the findMotifsGenome.pl software in Homer (V5.1).

Single-cell RNA sequencing and data analysis

Thymus from 5 mice for each group were pooled together, isolated thymocytes, and roughly enriched for CD25⁺ cells using magnetic beads. The scRNA-seq libraries were generated using the 10 \times Genomics Chromium Controller Instrument and Chromium Single Cell 3' V3 Reagent Kits (10 \times Genomics, Pleasanton, CA). Briefly, cells were concentrated to 1000 cells/ μ l and approximately 8000 cells were loaded into each channel to generate single-cell gel bead-in-emulsions (GEM), which results into expected mRNA barcoding of 5000 single-cells for each sample. After the RT step, GEMs were broken and barcoded-cDNA was purified and amplified. The amplified barcoded cDNA was fragmented, A-tailed, ligated with adaptors and index PCR amplified. The final libraries were quantified using the Qubit High Sensitivity DNA assay (Thermo Fisher Scientific) and the size distribution of the libraries were determined using a High Sensitivity DNA chip on a Bioanalyzer 2200 (Agilent). All libraries were sequenced by illumina sequencer (Illumina, San Diego, CA) on a 150 bp paired-end run.

scRNA-seq data analysis for CD4⁺ T cells was performed with NovelBrain Cloud Analysis Platform (www.novelbrain.com). Seurat package (version: 4.0.3, <https://satijalab.org/seurat/>) was used for cell normalization and regression based on the expression table according to the UMI counts of each sample and percent of mitochondria rate to obtain the scaled data. PCA was constructed based on the scaled data with top 2000 high variable genes and top 10 principals were used for tSNE construction and UMAP construction. Utilizing graph-based cluster method, the unsupervised cell cluster result based the PCA top 10 principal was acquired and the marker genes were calculated by FindAllMarkers function with Wilcox rank sum test algorithm under following criteria: 1. InFC > 0.25; 2. *p*-value < 0.05; 3. min.pct > 0.1. In order to identify the cell type detailed, the clusters of same cell type were selected for re-tSNE analysis, graph-based clustering and marker analysis. For pseudotime analysis, the Single-Cell Trajectories analysis utilizing Monocle2 (<http://cole-trapnell-lab.github.io/monocle-release>) using DDR-Tree and default parameter.

Based on the pseudo-time analysis, branch expression analysis modeling (BEAM Analysis) was applied for branch fate determined gene analysis.

Statistics

Data are given as means \pm SEM and analyzed with Prism version 6.0 (GraphPad Software). Data were analyzed by Student's *t*-test between two groups. Survival curves were compared by log-rank (Mantel-Cox) test. Differences were considered significant when *P* < 0.05.

Study approval

The mouse care and experimental protocols conducted in this study were approved by the Huazhong University of Science and Technology Animal Care and Use Committee.

Reporting summary

Further information on research design is available in the Nature Portfolio Reporting Summary linked to this article.

Data availability

Raw data files from bulk RNA-seq and CUT&Tag experiments have been deposited in the NCBI Sequence Read Archive (<https://www.ncbi.nlm.nih.gov/sra/>) under accession number PRJNA843698 (for bulk RNA-seq, <https://www.ncbi.nlm.nih.gov/bioproject/PRJNA843698>), and in the Gene Expression Omnibus (GEO) under accession number GSE288264 (CUT&Tag, <https://www.ncbi.nlm.nih.gov/geo/query/acc.cgi?acc=GSE288264>). The single-cell RNA-seq dataset has been deposited in GEO under accession number GSE225784. Source data are provided with this paper.

References

- Miller, J. F. Immunological function of the thymus. *Lancet* **2**, 748–749 (1961).
- Pantelouris, E. M. Observations on the immunobiology of ‘nude’ mice. *Immunology* **20**, 247–252 (1971).
- Bolton, E. M., Gracie, J. A., Briggs, J. D., Kampinga, J. & Bradley, J. A. Cellular requirements for renal allograft rejection in the athymic nude rat. *J. Exp. Med.* **169**, 1931–1946 (1989).
- Krieger, N. R., Yin, D. P. & Fathman, C. G. CD4⁺ but not CD8⁺ cells are essential for alloreactivity. *J. Exp. Med.* **184**, 2013–2018 (1996).
- Liu, Z., Fan, H. & Jiang, S. CD4⁺ T-cell subsets in transplantation. *Immunol. Rev.* **252**, 183–191 (2013).
- van Gelder, T., van Schaik, R. H. & Hesselink, D. A. Pharmacogenetics and immunosuppressive drugs in solid organ transplantation. *Nat. Rev. Nephrol.* **10**, 725–731 (2014).
- Stallone, G. et al. Sirolimus for Kaposi's sarcoma in renal-transplant recipients. *N. Engl. J. Med.* **352**, 1317–1323 (2005).
- Wu, X. et al. Opposing roles for calcineurin and ATF3 in squamous skin cancer. *Nature* **465**, 368–372 (2010).
- Dantal, J. & Souillou, J. P. Immunosuppressive drugs and the risk of cancer after organ transplantation. *N. Engl. J. Med.* **352**, 1371–1373 (2005).
- Roberts, M. B. & Fishman, J. A. Immunosuppressive agents and infectious risk in transplantation: managing the “Net State of Immunosuppression”. *Clin. Infect. Dis.* **73**, e1302–e1317 (2021).
- Sakaguchi, S., Miyara, M., Costantino, C. M. & Hafler, D. A. FOXP3⁺ regulatory T cells in the human immune system. *Nat. Rev. Immunol.* **10**, 490–500 (2010).
- Atif, M., Cherai, M. & Miyara, M. Phenotypic and functional studies of human Treg cell subpopulations. *Methods Mol. Biol.* **2559**, 153–169 (2023).
- Hall, B. M., Pearce, N. W., Gurley, K. E. & Dorsch, S. E. Specific unresponsiveness in rats with prolonged cardiac allograft survival after treatment with cyclosporine. III. Further characterization of the

- CD4+ suppressor cell and its mechanisms of action. *J. Exp. Med.* **171**, 141–157 (1990).
14. Issa, F., Robb, R. J. & Wood, K. J. The where and when of T cell regulation in transplantation. *Trends Immunol.* **34**, 107–113 (2013).
 15. Fan, H. et al. Regulatory T cell therapy for the induction of clinical organ transplantation tolerance. *Semin. Immunol.* **23**, 453–461 (2011).
 16. Field, E. H. et al. CD4+CD25+ regulatory cells in acquired MHC tolerance. *Immunol. Rev.* **182**, 99–112 (2001).
 17. Wing, J. B., Tanaka, A. & Sakaguchi, S. Human FOXP3(+) regulatory T cell heterogeneity and function in autoimmunity and cancer. *Immunity* **50**, 302–316 (2019).
 18. Zhang, R., Miao, J. & Zhu, P. Regulatory T cell heterogeneity and therapy in autoimmune diseases. *Autoimmun. Rev.* **20**, 102715 (2021).
 19. Li, X., Liang, Y., LeBlanc, M., Benner, C. & Zheng, Y. Function of a Foxp3 cis-element in protecting regulatory T cell identity. *Cell* **158**, 734–748 (2014).
 20. Feng, Y. et al. Control of the inheritance of regulatory T cell identity by a cis element in the Foxp3 locus. *Cell* **158**, 749–763 (2014).
 21. Zheng, Y. et al. Role of conserved non-coding DNA elements in the Foxp3 gene in regulatory T-cell fate. *Nature* **463**, 808–812 (2010).
 22. Ohkura, N. & Sakaguchi, S. Transcriptional and epigenetic basis of Treg cell development and function: its genetic anomalies or variations in autoimmune diseases. *Cell Res* **30**, 465–474 (2020).
 23. Ohkura, N. et al. T cell receptor stimulation-induced epigenetic changes and Foxp3 expression are independent and complementary events required for Treg cell development. *Immunity* **37**, 785–799 (2012).
 24. Padeken, J., Methot, S. P. & Gasser, S. M. Establishment of H3K9-methylated heterochromatin and its functions in tissue differentiation and maintenance. *Nat. Rev. Mol. Cell Biol.* **23**, 623–640 (2022).
 25. Adoue, V. et al. The histone methyltransferase SETDB1 controls T helper cell lineage integrity by repressing endogenous retroviruses. *Immunity* **50**, 629–644.e628 (2019).
 26. Xiao, X. et al. The costimulatory receptor OX40 inhibits interleukin-17 expression through activation of repressive chromatin remodeling pathways. *Immunity* **44**, 1271–1283 (2016).
 27. Ford, M. L. T cell cosignaling molecules in transplantation. *Immunity* **44**, 1020–1033 (2016).
 28. Rowe, H. M. et al. De novo DNA methylation of endogenous retroviruses is shaped by KRAB-ZFPs/KAP1 and ESET. *Development* **140**, 519–529 (2013).
 29. Quenneville, S. et al. In embryonic stem cells, ZFP57/KAP1 recognize a methylated hexanucleotide to affect chromatin and DNA methylation of imprinting control regions. *Mol. Cell* **44**, 361–372 (2011).
 30. Griffin, G. K. et al. Epigenetic silencing by SETDB1 suppresses tumour intrinsic immunogenicity. *Nature* **595**, 309–314 (2021).
 31. Bieber, C. P., Reitz, B. A., Jamieson, S. W., Oyer, P. E. & Stinson, E. B. Malignant lymphoma in cyclosporin A treated allograft recipients. *Lancet* **1**, 43 (1980).
 32. Leigh, I. M. & Glover, M. T. Cutaneous warts and tumours in immunosuppressed patients. *J. R. Soc. Med.* **88**, 61–62 (1995).
 33. Sanchez-Fueyo, A. & Strom, T. B. Immunologic basis of graft rejection and tolerance following transplantation of liver or other solid organs. *Gastroenterology* **140**, 51–64 (2011).
 34. Tantravahi, J., Womer, K. L. & Kaplan, B. Why hasn't eliminating acute rejection improved graft survival? *Annu. Rev. Med.* **58**, 369–385 (2007).
 35. Kaspruwicz, D. J., Smallwood, P. S., Tyznik, A. J. & Ziegler, S. F. Scurfin (FoxP3) controls T-dependent immune responses in vivo through regulation of CD4+ T cell effector function. *J. Immunol.* **171**, 1216–1223 (2003).
 36. Hori, S., Nomura, T. & Sakaguchi, S. Control of regulatory T cell development by the transcription factor Foxp3. *Science* **299**, 1057–1061 (2003).
 37. Fontenot, J. D., Gavin, M. A. & Rudensky, A. Y. Foxp3 programs the development and function of CD4+CD25+ regulatory T cells. *Nat. Immunol.* **4**, 330–336 (2003).
 38. Josefowicz, S. Z., Lu, L. F. & Rudensky, A. Y. Regulatory T cells: mechanisms of differentiation and function. *Annu. Rev. Immunol.* **30**, 531–564 (2012).
 39. Kanamori, M., Nakatsukasa, H., Okada, M., Lu, Q. & Yoshimura, A. Induced regulatory T cells: their development, stability, and applications. *Trends Immunol.* **37**, 803–811 (2016).
 40. Miragaia, R. J. et al. Single-cell transcriptomics of regulatory T cells reveals trajectories of tissue adaptation. *Immunity* **50**, 493–504.e497 (2019).
 41. Campbell, D. J. MyD88 and IL-1: loosening T(reg) cells' firm grip. *Trends Immunol.* **35**, 95–96 (2014).
 42. Li, M. O. & Rudensky, A. Y. T cell receptor signalling in the control of regulatory T cell differentiation and function. *Nat. Rev. Immunol.* **16**, 220–233 (2016).
 43. Hsieh, C. S., Lee, H. M. & Lio, C. W. Selection of regulatory T cells in the thymus. *Nat. Rev. Immunol.* **12**, 157–167 (2012).
 44. Corry, R. J., Winn, H. J. & Russell, P. S. Primarily vascularized allografts of hearts in mice. The role of H-2D, H-2K, and non-H-2 antigens in rejection. *Transplantation* **16**, 343–350 (1973).

Acknowledgements

We thank Dr. Deborah McClellan for editorial assistance. This work was supported by National Natural Science Foundation of China (82071771, 82271807 to P.L.; 82001700, to X.T.), and the Non-Profit Central Research Institute Fund of Chinese Academy of Medical Sciences (2023-PT320-07 to P.L.).

Author contributions

P.L., G.C., and Z.C. conceived and supervised the project. X.T., X.Z., D.J., Z.M., L.S., J.W., X.H., B.X., C.W., and S.Z. performed the in vitro and in vivo experiments. X.T., Z.H., M.W., M.M., and L.C. conducted the data analyses. P.L., X.T., G.C., and Z.C. wrote the paper. All authors read and approved the final paper.

Competing interests

The authors declare no competing interests.

Additional information

Supplementary information The online version contains supplementary material available at <https://doi.org/10.1038/s41467-025-58841-z>.

Correspondence and requests for materials should be addressed to Zhishui Chen, Gang Chen or Peixiang Lan.

Peer review information *Nature Communications* thanks the anonymous reviewer(s) for their contribution to the peer review of this work. A peer review file is available.

Reprints and permissions information is available at <http://www.nature.com/reprints>

Publisher's note Springer Nature remains neutral with regard to jurisdictional claims in published maps and institutional affiliations.

Open Access This article is licensed under a Creative Commons Attribution-NonCommercial-NoDerivatives 4.0 International License, which permits any non-commercial use, sharing, distribution and reproduction in any medium or format, as long as you give appropriate credit to the original author(s) and the source, provide a link to the Creative Commons licence, and indicate if you modified the licensed material. You do not have permission under this licence to share adapted material derived from this article or parts of it. The images or other third party material in this article are included in the article's Creative Commons licence, unless indicated otherwise in a credit line to the material. If material is not included in the article's Creative Commons licence and your intended use is not permitted by statutory regulation or exceeds the permitted use, you will need to obtain permission directly from the copyright holder. To view a copy of this licence, visit <http://creativecommons.org/licenses/by-nc-nd/4.0/>.

© The Author(s) 2025

¹Institute of Organ Transplantation, Tongji Hospital, Tongji Medical College, Huazhong University of Science and Technology, 430030 Wuhan, People's Republic of China. ²Key Laboratory of Organ Transplantation, Ministry of Education; NHC Key Laboratory of Organ Transplantation; Key Laboratory of Organ Transplantation, Chinese Academy of Medical Sciences, 430030 Wuhan, People's Republic of China. ³Department of Computational and Quantitative Medicine, Beckman Research Institute of City of Hope, Duarte, CA, USA. ⁴Department of Systems Biology, Beckman Research Institute of City of Hope, Duarte, CA 91016, USA. ⁵Division of Cardiothoracic and Vascular Surgery, Tongji Hospital, Tongji Medical College, Huazhong University of Science and Technology, 430030 Wuhan, People's Republic of China. ⁶Department of Immunology, School of Basic Medicine, Tongji Medical College, Huazhong University of Science and Technology, 430030 Wuhan, People's Republic of China. ⁷School of Medicine, South China University of Technology, 510000 Guangzhou, People's Republic of China. ⁸Department of Respiratory and Critical Care Medicine, the Center for Biomedical Research, NHC Key Laboratory of Respiratory Diseases, Tongji Hospital, Tongji Medical College, Huazhong University of Science and Technology, 430030 Wuhan, People's Republic of China. ⁹Department of Thyroid and Breast Surgery, Tongji Hospital, Tongji Medical College, Huazhong University of Science and Technology, 430030 Wuhan, People's Republic of China. ¹⁰These authors contributed equally: Xiaosheng Tan, Xiangli Zhao. ✉e-mail: zschen@tjh.tjmu.edu.cn; gchen@tjh.tjmu.edu.cn; lan-song9783@126.com